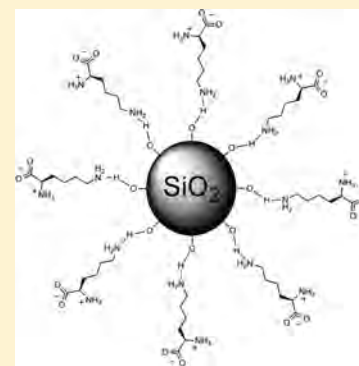


## Investigating Lysine Adsorption on Fumed Silica Nanoparticles

Chengchen Guo<sup>†</sup> and Gregory P. Holland<sup>\*,‡</sup><sup>†</sup>Department of Chemistry and Biochemistry, Magnetic Resonance Research Center, Arizona State University, Tempe, Arizona 85287-1604, United States<sup>‡</sup>Department of Chemistry and Biochemistry, San Diego State University, 5500 Campanile Drive, San Diego, California 92182-1030, United States

## S Supporting Information

**ABSTRACT:** The adsorption of amino acids on silica surfaces has attracted considerable interest because it has a broad range of applications in various fields such as drug delivery, solid-phase peptide synthesis, and biocompatible materials synthesis. In this work, we systematically study lysine adsorption on fumed silica nanoparticles with thermal analysis and solid-state NMR. Thermogravimetric analysis results show that the adsorption behavior of lysine in low-concentration aqueous solutions is well-described by the Langmuir isotherm. With ultrafast magic-angle-spinning <sup>1</sup>H NMR and multinuclear and multidimensional <sup>13</sup>C and <sup>15</sup>N solid-state NMR, we successfully determine the protonation state of bulk lysine and find that lysine is adsorbed on silica nanoparticle surfaces through the side-chain amine groups. Density functional theory calculations carried out on lysine and lysine–silanol complex structures further confirm that the side-chain amine groups interact with the silica surface hydroxyl groups via strong hydrogen bonding. Furthermore, we find that lysine preferentially has monolayer coverage on silica surfaces in high salt concentration solutions because of the ionic complexes formed with surface bound lysine molecules.



## ■ INTRODUCTION

The nature of interactions between biomolecules and the surfaces of inorganic materials has attracted considerable attention because it is of great significance in many promising fields, such as prebiotic chemistry,<sup>1–3</sup> bionanotechnology,<sup>4–9</sup> and drug delivery.<sup>10–14</sup> For instance, some minerals have been shown to catalyze peptide synthesis, providing a new explanation on the origin of life.<sup>2,15</sup> In addition, some biomolecules with pharmaceutical properties can be adsorbed at specific inorganic material interfaces and then released in vivo in a well-controlled way.<sup>11,14</sup> Adsorption of amino acids and peptides on silica surfaces is one specific class of such bioorganic–inorganic interface systems. Silica was extensively studied and utilized for various applications such as catalysis, solar cells, and even cancer therapy.<sup>4,11,16</sup> Fumed silica is one class of synthetic silica materials with a high surface area.<sup>17</sup> It is produced at high temperature by hydrolyzing silicon tetrachloride vapor in a flame followed by rapid quenching to room temperature. Because of this, it acquires some unique characteristics such as amorphous structure, nanoscale size, and an extensively high surface area. The studies of surface chemistry at fumed silica interfaces have been carried out for decades because of the considerable utility of high surface area amorphous silicates.<sup>17–25</sup>

Lysine (Lys) has been used in a large number of studies because of its unique structure, where there is one single side-chain amine group. It is this side-chain amine group that makes lysine the simplest basic amino acid compared with the other two basic amino acids, arginine and histidine. Because of this, lysine has been used in synthesizing a range of nanomateri-

als.<sup>26–28</sup> Recently, Yokoi et al. discovered that lysine is a good ligand in synthesizing ultrasmall silica nanoparticles (<10 nm) that show great potential in future nanotechnology applications.<sup>27</sup> Figure 1 shows the summary of different L-lysine forms and the charged state of a silica surface at variable pH values.<sup>29–31</sup> The structure of bulk lysine has not been clearly defined, but the structure of lysine monohydrochloride dihydrate was determined by X-ray diffraction (XRD) and neutron scattering techniques.<sup>32,33</sup>

Considerable work has been done to understand the interaction between amino acids and silica surfaces where the focus was on alanine and glycine adsorption.<sup>34–40</sup> Considerably less work has been performed to study lysine adsorption on silica surfaces.<sup>41–43</sup> The main techniques that have been used to study the adsorption behavior of lysine on surfaces of inorganic materials are infrared (IR) spectroscopy and thermal analysis. By using IR spectroscopy, it is easy to determine the protonation state of lysine on surfaces at variable pH values.<sup>31,41</sup> Thermal analysis, including thermogravimetric analysis (TGA) and differential scanning calorimetry (DSC), has also been applied to study the thermal transformation of lysine molecules on surfaces.<sup>38</sup> To date, solid-state NMR techniques have not been used to study lysine adsorption and thermal transformation of lysine molecules at silica interfaces. Compared with thermal analysis, solid-state NMR is able to provide molecular and atomic-level details.<sup>44</sup> Many solid-state

Received: August 26, 2014

Revised: October 8, 2014

Published: October 10, 2014

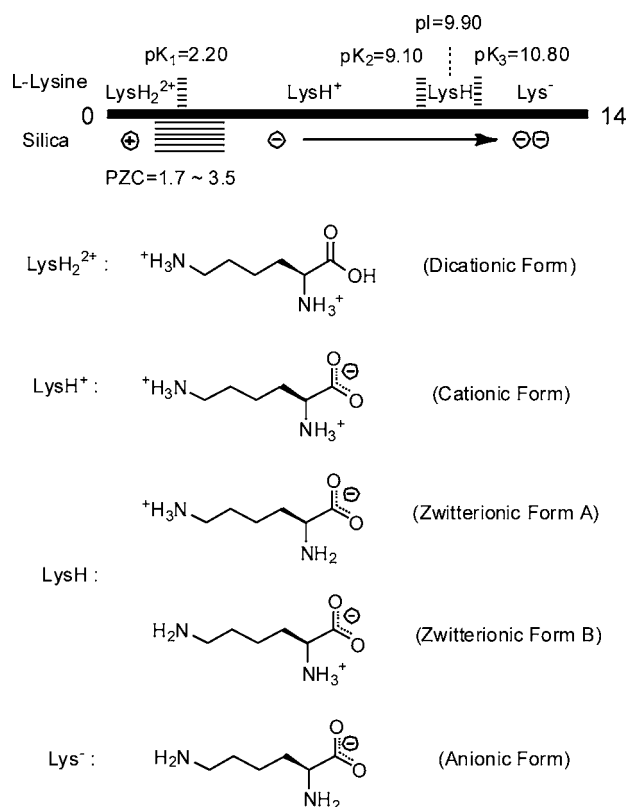


**Figure 1.** Summary of different L-lysine forms and charged states of silica surface as a function of pH values.<sup>41</sup>

NMR methods and techniques have been developed and applied to study the interaction between amino acids and silica surfaces.<sup>34–37,45–48</sup> Schmidt et al. used rotational-echo double-resonance (REDOR) NMR to investigate the adsorbed state and the local dynamics of alanine molecules on silica surface, and they proposed that alanine is more mobile when hydrated.<sup>45</sup> Also, Vega et al. used <sup>2</sup>H NMR to study the dynamics of water and alanine molecules adsorbed on silica surfaces.<sup>36</sup>

In the present work, we applied solid-state NMR techniques including ultrafast magic-angle-spinning<sup>49</sup> (MAS) <sup>1</sup>H NMR and multinuclear and multidimensional <sup>13</sup>C and <sup>15</sup>N NMR to determine the structure of bulk lysine and investigate lysine adsorbed on fumed silica nanoparticles.<sup>50,51</sup> Furthermore, to elucidate the interaction between lysine and silanol groups on silica surfaces, we performed density functional theory<sup>52,53</sup> (DFT) calculations for <sup>1</sup>H, <sup>13</sup>C, and <sup>15</sup>N chemical shifts of lysine–silanol complex species and geometries. The combination of NMR experiments with DFT calculations allows us to propose structural models for lysine interacting at silica nanoparticle interfaces.

## EXPERIMENTAL SECTION

**Materials.** Fumed silica nanoparticles (~7 nm) with Brunauer, Emmett, and Teller (BET) surface area of 395 ± 25 m<sup>2</sup>/g and pure L-lysine (99% purity) were purchased from Sigma-Aldrich. U-[<sup>15</sup>N,<sup>13</sup>C]-L-lysine-2HCl was purchased from Cambridge Isotopes, Inc. All materials were used as received, and the stable isotope enrichment levels of labeled compounds are 98%. U-[<sup>15</sup>N,<sup>13</sup>C]-L-lysine-2NaCl was prepared by crystallizing in deionized (DI) water after adjusting to pH ~ 10 with 1.0 M NaOH.

**Sample Preparation.** Fumed silica nanoparticles used in the study were initially heated up to 500 °C for 24 h to remove free water and impurities on the surface. In a typical adsorption procedure, 150 mg of fumed silica nanoparticles was immersed in a 10.0 mL of aqueous solution of L-lysine with varying concentrations, and the solution was stirred at room temperature for 3 h to ensure the adsorption reached equilibrium. The solid was then separated by centrifugation and carefully dried under vacuum at 30 °C for over 15 h. The samples prepared from solutions of various concentrations were noted as Lys/SiO<sub>2</sub>-xM, where *x* refers to the lysine concentration in the adsorption solution (in moles per liter). Because all experiments were carried out in pure DI water, the pH values of all the solutions are around 10.0 (10.0 ± 0.3), corresponding to the isoelectric pH value of lysine in pure water.

To prepare <sup>13</sup>C,<sup>15</sup>N-L-lysine adsorbed fumed silica samples, 60.0 mg of fumed silica nanoparticles and 9.0 mg of <sup>13</sup>C,<sup>15</sup>N-L-lysine-2HCl (0.01 M) were mixed in DI water, and the solution pH was adjusted to 10.0 with 1.0 M NaOH. The volume of the final solution is 4.0 mL, and the suspension was then stirred for 3 h to reach equilibrium. The mixture was then centrifuged, and the remaining powder was allowed to vacuum-dry at 30 °C for over 15 h.

**Thermogravimetric Analysis.** TGA experiments were performed on Lys/SiO<sub>2</sub>-xM samples with a TA2910 (TA Instrument Inc.) under N<sub>2</sub> flow (60 mL/min for furnace and 40 mL/min for balance). The heating rate was 5 °C/min, and for each experiment, 7–10 mg of the sample was used. Before each experiment, the sample was kept under a N<sub>2</sub> flow for 10 min to remove most of the physisorbed water and obtain a stable baseline.

**Solid-State NMR Spectroscopy.** <sup>1</sup>H → <sup>13</sup>C and <sup>1</sup>H → <sup>15</sup>N cross-polarization magic-angle-spinning<sup>54,55</sup> (CP-MAS) NMR experiments, two-dimensional (2D) <sup>13</sup>C–<sup>13</sup>C through-space correlation NMR experiments with dipolar-assisted rotational resonance<sup>56,57</sup> (DARR), 2D <sup>13</sup>C–<sup>13</sup>C through-bond double-quantum (DQ)/single-quantum (SQ) refocused incredible natural abundance double-quantum transfer NMR experiments<sup>58,59</sup> (INADEQUATE), and 2D <sup>15</sup>N–<sup>13</sup>C heteronuclear correlation (HETCOR) NMR experiments were performed on a Varian VNMRs 400 MHz spectrometer. For the U-[<sup>15</sup>N,<sup>13</sup>C]-L-lysine-2HCl and natural abundance Lys/SiO<sub>2</sub> samples, 2D <sup>13</sup>C–<sup>13</sup>C correlation experiments and CP-MAS NMR experiments were collected with a 4.0 mm triple-resonance probe operating in triple-resonance (<sup>1</sup>H/<sup>13</sup>C/<sup>15</sup>N) mode at a MAS speed of 10 kHz. The CP condition for <sup>1</sup>H → <sup>13</sup>C CP-MAS NMR experiments consisted of a 4.0 μs <sup>1</sup>H π/2 pulse followed by a 2.0 ms ramped (8%) <sup>1</sup>H spin-lock pulse of 62.5 kHz radio frequency (rf) field strength. The experiments were performed with a 50 kHz sweep width, a recycle delay of 3.0 s, and two-pulse phase-modulated<sup>60</sup> (TPPM) <sup>1</sup>H decoupling level of 65 kHz. The CP condition for <sup>1</sup>H → <sup>15</sup>N CP-MAS NMR experiments consisted of a 3.25 μs <sup>1</sup>H π/2 pulse followed by a 1.0 ms ramped (10%) <sup>1</sup>H spin-lock pulse of 75 kHz rf field strength. The experiments were performed with a 50 kHz sweep width, a recycle delay of 3.0 s, and <sup>1</sup>H decoupling level of 80 kHz. For the <sup>13</sup>C,<sup>15</sup>N-labeled Lys/SiO<sub>2</sub> samples, CP-MAS NMR experiments and 2D <sup>15</sup>N–<sup>13</sup>C HETCOR NMR experiments were collected with a 3.2 mm triple-resonance probe operating in triple-resonance (<sup>1</sup>H/<sup>13</sup>C/<sup>15</sup>N) mode at a MAS speed of 10 kHz. For <sup>1</sup>H → <sup>13</sup>C CP-MAS NMR experiments, the CP condition consisted of a 2.5 μs <sup>1</sup>H π/2 pulse, followed by a 1.0 ms ramped (8%) <sup>1</sup>H spin-lock pulse of 100 kHz rf field

strength. The experiments were performed with a 50 kHz sweep width, a recycle delay of 3.0 s, and  $^1\text{H}$  decoupling level of 90 kHz. For  $^1\text{H} \rightarrow ^{15}\text{N}$  CP-MAS NMR experiments, the CP condition consisted of  $2.5 \mu\text{s}$   $^1\text{H}$   $\pi/2$  pulse, followed by a 1.0 ms ramped (12%)  $^1\text{H}$  spin-lock pulse of 55 kHz rf field strength. The experiments were performed with a 25 kHz sweep width, a recycle delay of 5.0 s, and  $^1\text{H}$  decoupling level of 90 kHz. 2D  $^{13}\text{C}$ – $^{13}\text{C}$  through-space correlation NMR experiments, 2D  $^{13}\text{C}$ – $^{13}\text{C}$  INADEQUATE, and 2D  $^{15}\text{N}$ – $^{13}\text{C}$  HETCOR NMR experiments were used for assigning resonances (see Supporting Information for data and experimental details).

$^1\text{H}$  MAS NMR experiments and 2D  $^1\text{H}$ – $^{13}\text{C}$  HETCOR NMR experiments were carried out on a Varian VNMRs 800 MHz instrument with a 1.6 mm triple-resonance probe operating in double-resonance ( $^1\text{H}/^{13}\text{C}$ ) mode.  $^1\text{H}$  MAS NMR experiments were collected with  $2.0 \mu\text{s}$   $^1\text{H}$   $\pi/2$  pulse, 25 kHz sweep width at 30 kHz MAS. 2D  $^1\text{H}$ – $^{13}\text{C}$  HETCOR NMR experiments were done at a spinning speed of 35 kHz. The  $^1\text{H} \rightarrow ^{13}\text{C}$  CP condition consisted of a  $2.6 \mu\text{s}$   $^1\text{H}$   $\pi/2$  pulse, followed by a ramped (10%)  $^1\text{H}$  spin-lock pulse of 100 kHz rf field strength of variable contact time (0.25 ms, 2.0 ms). The sweep widths of direct dimension and indirect dimension are 50 kHz and 25 kHz, respectively, with 32 complex  $t_1$  points. The recycle delay was 3.0 s, and TPPM  $^1\text{H}$  decoupling with a rf field strength of 110 kHz was used during acquisition.

Ultrafast  $^1\text{H}$  MAS NMR experiments and  $^1\text{H}$ – $^1\text{H}$  back-to-back<sup>61–63</sup> (BABA) dipolar DQ/SQ correlation NMR experiments were carried out on a Bruker AVIII 850 MHz spectrometer equipped with a 1.3 mm double-resonance probe ( $^1\text{H}/^{13}\text{C}$ ) at a MAS speed of 67 kHz. The experiments were done with one rotor period BABA for excitation and reconversion, a  $1.5 \mu\text{s}$   $^1\text{H}$   $\pi/2$  pulse, relaxation delay of 5.0 s, and 128 complex  $t_1$  points. In all experiments, the chemical shifts of  $^1\text{H}$ ,  $^{13}\text{C}$ , and  $^{15}\text{N}$  were indirectly referenced to adamantane  $^1\text{H}$  (1.63 ppm), adamantane  $^{13}\text{C}$  (38.6 ppm), and glycine  $^{15}\text{N}$  (31.6 ppm), respectively.<sup>64,65</sup>

**DFT Calculation.** Both geometry optimization and NMR chemical shifts calculation were performed with the B3LYP DFT method using 6-31G+(d, p) basis sets in Gaussian09.<sup>66</sup> It is well-demonstrated that the B3LYP/6-31G+(d, p) level can provide reliable NMR chemical shift results.<sup>67–69</sup> To reduce the computational cost, we used a silanol (HOSiH<sub>3</sub>) molecule instead of using a complete silica surface model. In the calculations, bulk lysine and lysine–silanol complex species (Figure 2a,b) were geometrical optimized first, and then the optimized structures were used in NMR chemical shift calculations. NMR chemical shift calculations were performed using the gauge-including atomic orbital<sup>70,71</sup> method, and  $^1\text{H}$ ,  $^{13}\text{C}$ , and  $^{15}\text{N}$  chemical shift values were analyzed. In  $^{13}\text{C}$  and  $^{15}\text{N}$  data analysis, we applied two extrapolated curves for  $^{13}\text{C}$  and  $^{15}\text{N}$ , respectively, to transform all calculated chemical shielding values to chemical shift values. This method is demonstrated to be more accurate than simply using a standard reference.<sup>67,68</sup> For  $^1\text{H}$ , the calculated chemical shifts were referenced to  $^1\text{H}$  chemical shift of tetramethylsilane calculated with the same basis set.

## RESULTS AND DISCUSSION

**Protonation State of L-Lysine in the Solid State.** The  $^1\text{H}$  MAS NMR spectra of natural abundance bulk lysine at different MAS speeds are shown in Figure 3A, and the 2D

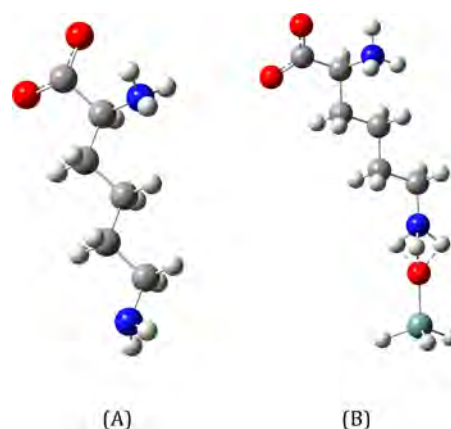


**Figure 2.** Bulk lysine and lysine–silanol complex models used in DFT calculations: (A) lysine and (B) Lys–H–OSiH<sub>3</sub>.

$^1\text{H}$ – $^1\text{H}$  dipolar DQ/SQ NMR spectrum collected with the BABA pulse sequence is shown in Figure 3B. With increasing spinning speed, the resolution of the  $^1\text{H}$  MAS NMR spectrum for bulk lysine is improved dramatically with well-resolved resonances observed for the spectrum collected with a 67 kHz MAS speed. According to 2D  $^1\text{H}$ – $^{13}\text{C}$  HETCOR NMR spectrum (Figure S1 of Supporting Information), the resonances at 3.6 and 2.2 ppm were assigned to  $\alpha$ -CH and  $\epsilon$ -CH<sub>2</sub>, respectively, and the broad component at 1.5 ppm is a combination of  $\beta$ -CH<sub>2</sub>,  $\gamma$ -CH<sub>2</sub>, and  $\delta$ -CH<sub>2</sub>. It is difficult to determine the protonation states of the amine groups in bulk lysine from the  $^1\text{H}$  MAS and 2D  $^1\text{H}$ – $^{13}\text{C}$  HETCOR NMR experiments. A  $^1\text{H}$ – $^1\text{H}$  DQ/SQ NMR experiment with a MAS speed of 67 kHz was applied to better assign the  $^1\text{H}$  spectrum. In the  $^1\text{H}$ – $^1\text{H}$  DQ/SQ NMR spectrum, the resonance at 3.6 ppm was assigned to  $\alpha$ -CH because it has no on-diagonal resonance, and this result is consistent with the 2D  $^1\text{H}$ – $^{13}\text{C}$  HETCOR NMR result. The resonance at 8.4 ppm was assigned to  $\alpha$ -NH<sub>3</sub><sup>+</sup> because only strong DQ correlation to  $\alpha$ -CH was observed with no obvious DQ correlation to  $\epsilon$ -CH<sub>2</sub> (dashed circle in Figure 3B). The result indicates that  $\epsilon$ -NH<sub>2</sub> is not protonated in bulk lysine and it has a relatively small resonance that is probably convoluted by the broad component in the 0–2 ppm region of the spectrum. DFT calculation further suggests that the  $\epsilon$ -NH<sub>2</sub> resonance probably appears around 0.7 ppm. The protonation state of lysine in its bulk form is as proposed in Figure 3A and takes on the zwitterion form observed for most amino acids such as alanine and glycine.

**Adsorption Behavior of Lysine on Fumed Silica Nanoparticles.** TGA is an accurate technique for measuring the amount of adsorbed lysine on fumed silica nanoparticles. Because all adsorbed amino acids will completely decompose when heated to 600 °C under nitrogen gas flow, we can quantify the amount of lysine on the surface from TGA curves. Figure 4A shows the TGA curves for lysine/silica samples prepared from solutions with different initial lysine concentrations. Clearly, with increasing initial concentration, the surface coverage increases. The weight loss between 100 and 600 °C is attributed to the amount of lysine on the surfaces, and the quantitative results are presented in Table 1. As expected, the results show that the adsorbed amount of lysine increases when increasing the initial lysine concentration in solution. The adsorption behavior of lysine molecules is described in Figure 4B. We applied a Langmuir isotherm to fit the data, showing that at low concentration, the adsorption

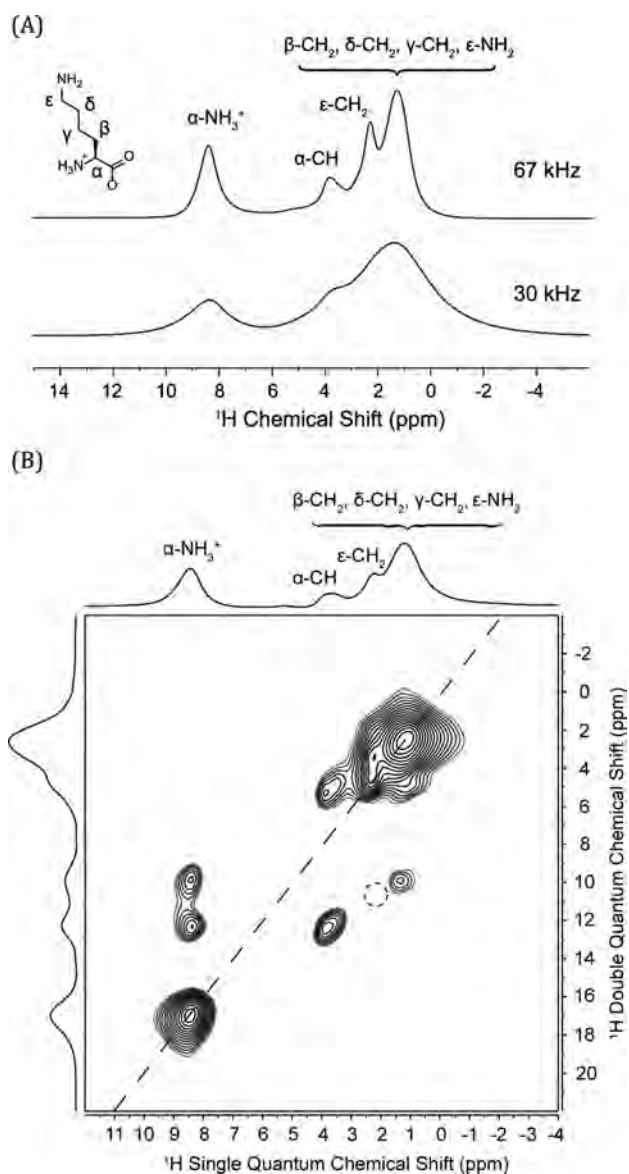


**Figure 3.** (A)  $^1\text{H}$  NMR spectra of natural abundance bulk lysine at MAS speeds of 30 kHz and 67 kHz at a  $^1\text{H}$  Larmor frequency of 800 and 850 MHz, respectively. (B)  $^1\text{H}$ - $^1\text{H}$  BABA NMR spectrum of natural abundance bulk lysine at spinning speed of 67 kHz at a  $^1\text{H}$  Larmor frequency of 850 MHz.

behavior of lysine fits well to a Langmuir isotherm but the fitting deviates at high concentration (Figure 4B). This is mostly because at high concentration the adsorption behavior of lysine depends not only on the state of the surface but also on the interaction between lysine molecules. On the basis of the Langmuir isotherm fitting result for the first 5 points, ideally the maximum amount of adsorbed lysine is  $2.3 \pm 0.2$  molecule/ $\text{nm}^2$  and the equilibrium constant is  $32.2 \pm 8.6 \text{ M}^{-1}$ .

**Adsorption State of Lysine on Fumed Silica Nanoparticles.**  $^1\text{H} \rightarrow ^{13}\text{C}$  and  $^1\text{H} \rightarrow ^{15}\text{N}$  CP-MAS NMR experiments were applied in this work to investigate the adsorption state of lysine at interfaces of nanoparticles. Figure 5 shows the  $^1\text{H} \rightarrow ^{13}\text{C}$  and  $^1\text{H} \rightarrow ^{15}\text{N}$  CP-MAS NMR spectra of three different lysine samples and two lysine/silica samples. The  $^{13}\text{C}$  and  $^{15}\text{N}$  resonance assignments are shown in Table 2. On the basis of the carbon and nitrogen NMR spectra and Table 2, several conclusions can be drawn. First, lysine has

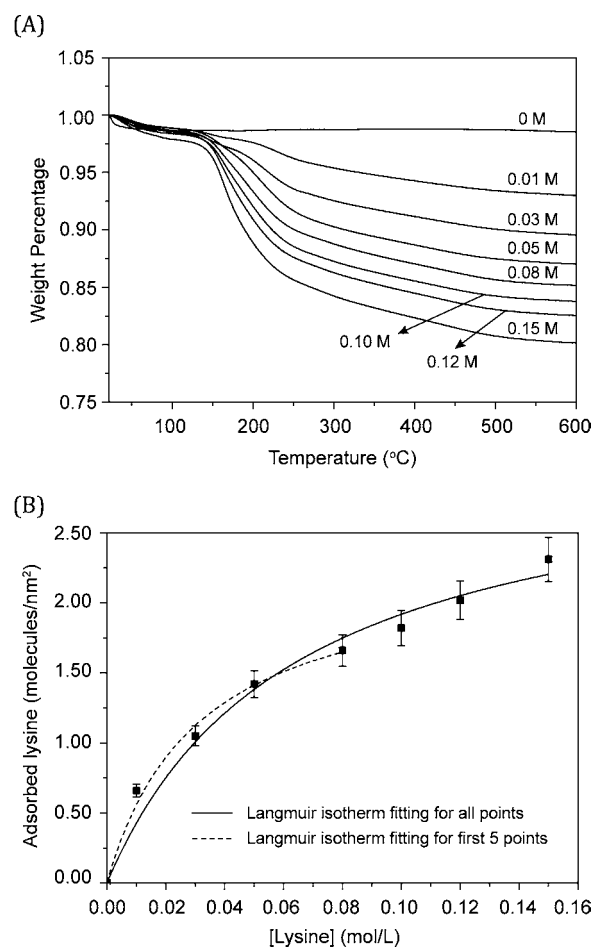


**Figure 4.** (A) TGA curves of lysine/silica samples as a function of initial concentration of lysine in the adsorption solution. (B) Amount of lysine adsorbed on silica as a function of initial concentration of lysine at room temperature and pH 10.0.

**Table 1. Effect of Initial Concentration of Solution on Lysine Adsorption on Fumed Silica Nanoparticles from TGA**

[lysine]	free water (wt %)	lysine (wt %)	total adsorbed amount (wt %)	surface coverage (molecules/ $\text{nm}^2$ )
0.01 M	1.16	5.85	7.01	0.7
0.03 M	1.39	9.06	10.45	1.1
0.05 M	1.13	11.85	12.98	1.4
0.08 M	1.34	13.51	14.85	1.7
0.10 M	1.63	14.62	16.25	1.8
0.12 M	1.48	15.99	17.47	2.0
0.15 M	2.12	17.74	19.86	2.3

three different protonation states. For natural abundance lysine, it was shown from the 2D  $^1\text{H}$ - $^1\text{H}$  dipolar DQ/SQ NMR spectrum that the  $\epsilon\text{-NH}_2$  is deprotonated and the  $\alpha\text{-NH}_2$  is protonated (Figure 3). The  $^{13}\text{C}$  resonances at 177, 55, 35, 22, 32, and 44 ppm were assigned to carboxyl group,  $\alpha\text{-CH}$ ,  $\beta\text{-CH}$ ,  $\gamma\text{-CH}$ ,  $\delta\text{-CH}$ , and  $\epsilon\text{-CH}_2$ , respectively, and the  $^{15}\text{N}$  resonances at 39 and 24 ppm were assigned to  $\alpha\text{-NH}_3^+$  and  $\epsilon\text{-NH}_2$ , respectively, based on INADEQUATE and 2D  $^{15}\text{N}$ - $^{13}\text{C}$  HETCOR NMR experiments, respectively (Figures S2 and S3 of Supporting Information). For  $^{13}\text{C}$ , $^{15}\text{N}$ -lysine-2HCl, the  $^{15}\text{N}$  resonances of both amine groups have large downfield shifts due to protonation and hydrogen bonding interaction with  $\text{Cl}^-$ . In addition, the  $^{13}\text{C}$  resonance of the carboxyl group

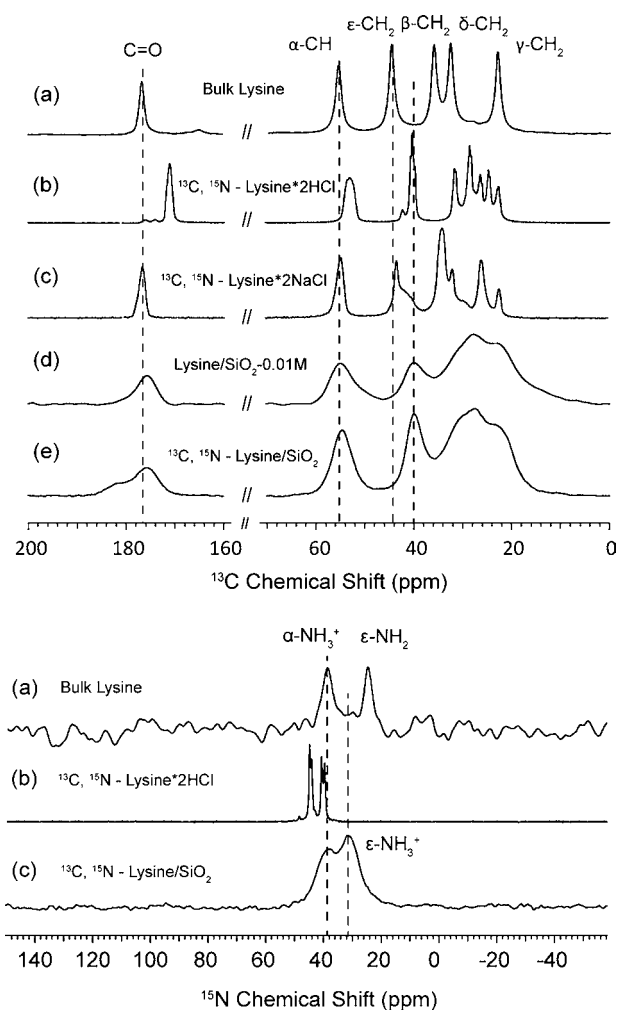


**Figure 5.** Top panel:  $^1\text{H} \rightarrow ^{13}\text{C}$  CP-MAS NMR spectra of (a) bulk lysine, (b)  $^{13}\text{C}, ^{15}\text{N}$ -lysine-2HCl, (c)  $^{13}\text{C}, ^{15}\text{N}$ -lysine-2NaCl, (d) Lys/SiO<sub>2</sub>-0.01 M, and (e)  $^{13}\text{C}, ^{15}\text{N}$ -lysine/SiO<sub>2</sub> (0.01 M). The spectra were collected with a MAS speed of 10 kHz, a relaxation delay time of 3 s, and a contact time of 1.0 ms. Bottom panel:  $^1\text{H} \rightarrow ^{15}\text{N}$  CP-MAS NMR spectra of (a) bulk lysine, (b)  $^{13}\text{C}, ^{15}\text{N}$ -lysine-2HCl and (c)  $^{13}\text{C}, ^{15}\text{N}$ -lysine/SiO<sub>2</sub> (0.01 M). The spectra were collected with a MAS speed of 10 kHz, a relaxation delay time of 3 s, and a contact time of 1.0 ms. Both  $^1\text{H} \rightarrow ^{13}\text{C}$  and  $^1\text{H} \rightarrow ^{15}\text{N}$  CP-MAS NMR experiments were carried out at a  $^1\text{H}$  Larmor frequency of 400 MHz with a 4.0 mm triple-resonance probe operating in triple-resonance ( $^1\text{H}/^{13}\text{C}/^{15}\text{N}$ ) mode and a 3.2 mm triple-resonance probe operating in triple-resonance ( $^1\text{H}/^{13}\text{C}/^{15}\text{N}$ ) mode, respectively.

shifts upfield by 6 ppm to 171 ppm, indicating that the carboxyl group is protonated. For  $^{13}\text{C}, ^{15}\text{N}$ -lysine-2NaCl, the  $^{13}\text{C}$

resonances of the carboxyl group and  $\alpha$ -CH are identical to those of natural abundance lysine, indicating the carboxyl group is deprotonated and the  $\alpha$ -NH<sub>2</sub> is protonated. However, two resonances are found in the  $\epsilon$ -CH<sub>2</sub> region with one at 40 ppm and the other at 43 ppm, indicating that there is a mixture of protonated and deprotonated components. The proposed structure of each sample is presented in Table 2.

When the lysine spectra are compared with the lysine/SiO<sub>2</sub> spectra, it is found that for both the Lys/SiO<sub>2</sub>-0.01 M and the  $^{13}\text{C}, ^{15}\text{N}$ -lysine/SiO<sub>2</sub>, the  $^{13}\text{C}$  resonances of the carboxyl group and  $\alpha$ -CH and the  $^{15}\text{N}$  resonance of  $\alpha$ -NH<sub>2</sub> are almost identical to those of natural abundance lysine, indicating the carboxyl group is deprotonated and the  $\alpha$ -NH<sub>2</sub> is protonated ( $\alpha$ -NH<sub>3</sub><sup>+</sup>). However, the  $^{13}\text{C}$  resonance of  $\epsilon$ -CH<sub>2</sub> has a value identical to that of  $^{13}\text{C}, ^{15}\text{N}$ -lysine-2HCl and the  $^{15}\text{N}$  resonance of  $\epsilon$ -NH<sub>2</sub> has an 8 ppm downfield shift compared with that of natural abundance lysine, indicating that the  $\epsilon$ -NH<sub>2</sub> is protonated, forming a strong hydrogen bonding interaction with the surface silanol groups. To prove this hypothesis, we further applied 2D  $^1\text{H}$ - $^{13}\text{C}$  HETCOR NMR experiments (Figure 7) to investigate the correlation between silanol groups and adsorbed lysine. The results of the HETCOR NMR experiment are discussed in the following paragraph. It is also worth mentioning that one extra resonance at 182 ppm is found in the carboxyl group region for  $^{13}\text{C}, ^{15}\text{N}$ -lysine/SiO<sub>2</sub>. This is probably due to a small amount of NaCl present in the sample, forming a lysine-NaCl complex.<sup>72</sup>

The  $^1\text{H}$  MAS spectra of natural abundance pure lysine and  $^{13}\text{C}, ^{15}\text{N}$ -lysine/SiO<sub>2</sub> at a MAS speed of 67 kHz are shown in Figure 6. It is found that  $^1\text{H}$  resonances of  $\alpha$ -CH and  $\epsilon$ -CH<sub>2</sub> for

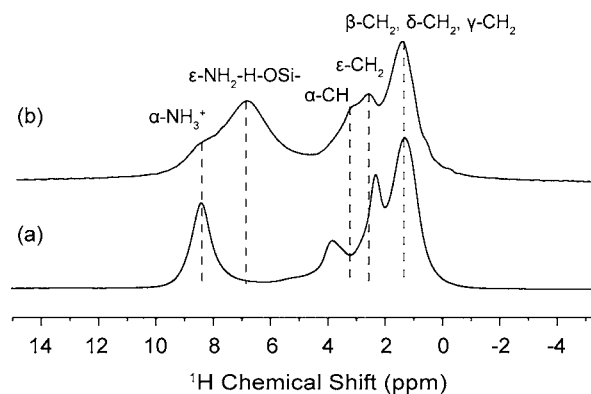


**Figure 6.**  $^1\text{H}$  NMR spectra of (a) natural abundance bulk lysine and (b)  $^{13}\text{C}, ^{15}\text{N}$ -lysine/SiO<sub>2</sub> at a MAS speed of 67 kHz. Spectra were collected at a  $^1\text{H}$  Larmor frequency of 850 MHz.

adsorbed lysine have small offsets compared to those of bulk lysine. This is probably due to the change of structure and

**Table 2.**  $^{13}\text{C}$  and  $^{15}\text{N}$  Chemical Shifts of Lysine and Lysine/SiO<sub>2</sub> Samples<sup>a</sup>

sample	C=O	C <sub>α</sub>	C <sub>β</sub>	C <sub>γ</sub>	C <sub>δ</sub>	C <sub>ε</sub>	$\alpha$ -NH <sub>2</sub> / $\alpha$ -NH <sub>3</sub> <sup>+</sup>	$\epsilon$ -NH <sub>2</sub> / $\epsilon$ -NH <sub>3</sub> <sup>+</sup>	structure
natural abundance lysine	177	55	35	22	32	44	39	24	NH <sub>2</sub> (CH <sub>2</sub> ) <sub>4</sub> CH(NH <sub>3</sub> <sup>+</sup> )COO <sup>-</sup>
$^{13}\text{C}, ^{15}\text{N}$ -lysine-2HCl	171	53	31, 26	21, 23	25, 26	40	45	40	Cl <sup>-</sup> NH <sub>3</sub> <sup>+</sup> (CH <sub>2</sub> ) <sub>4</sub> CH(NH <sub>3</sub> <sup>+</sup> Cl <sup>-</sup> )COOH
$^{13}\text{C}, ^{15}\text{N}$ -lysine-2NaCl	177	55	33	22	31, 25	43, 40	—	—	NH <sub>2</sub> (CH <sub>2</sub> ) <sub>4</sub> CH(NH <sub>3</sub> <sup>+</sup> )COO <sup>-</sup> Cl <sup>-</sup> NH <sub>3</sub> <sup>+</sup> (CH <sub>2</sub> ) <sub>4</sub> CH(NH <sub>3</sub> <sup>+</sup> )COO <sup>-</sup>
Lys/SiO <sub>2</sub> -0.01M	176	55	30	23	27	40	—	—	SiO <sup>-</sup> NH <sub>3</sub> <sup>+</sup> (CH <sub>2</sub> ) <sub>4</sub> CH(NH <sub>3</sub> <sup>+</sup> )COO <sup>-</sup>
$^{13}\text{C}, ^{15}\text{N}$ -lysine/SiO <sub>2</sub>	176, 182	55	30	23	27	40	39	32	SiO <sup>-</sup> NH <sub>3</sub> <sup>+</sup> (CH <sub>2</sub> ) <sub>4</sub> CH(NH <sub>3</sub> <sup>+</sup> )COO <sup>-</sup>

<sup>a</sup>Chemical shifts are reported in ppm.

protonation state during the adsorption. The broad resonance at around 7.0 ppm is assigned to the protonated amine groups ( $\epsilon\text{-NH}_3^+$ ) interacting with the surface silanol groups at the silica nanoparticle interface. Figure 7 shows the 2D  $^1\text{H}$ - $^{13}\text{C}$

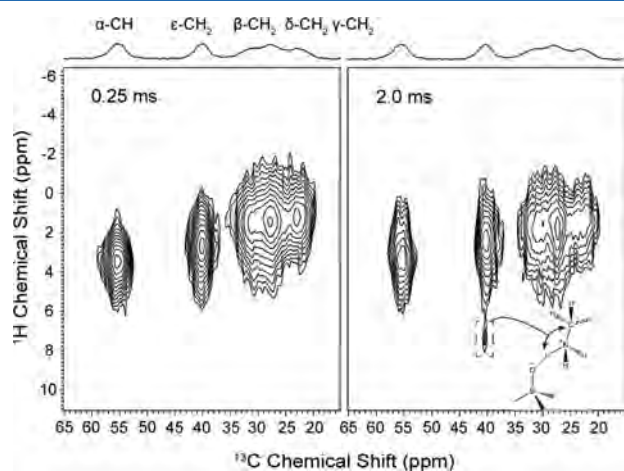


**Figure 7.**  $^1\text{H}$ - $^{13}\text{C}$  2D-HETCOR NMR spectrum of  $^{13}\text{C}$ ,  $^{15}\text{N}$ -lysine/ $\text{SiO}_2$  with different mixing times (0.25 ms, 2.0 ms). Experiments were done at a  $^1\text{H}$  Larmor frequency of 800 MHz with a 1.6 mm triple-resonance probe operating in double-resonance ( $^1\text{H}/^{13}\text{C}$ ) mode and a MAS speed of 35 kHz.

HETCOR NMR spectrum of  $^{13}\text{C}$ ,  $^{15}\text{N}$ -lysine/ $\text{SiO}_2$  with different CP contact times (0.25 ms, 2.0 ms). Because the 2D  $^1\text{H}$ - $^{13}\text{C}$  HETCOR NMR experiment is a dipolar-based experiment, in which magnetization is transferred through space, long-range correlations can be detected by applying a relatively long CP contact time. In addition to seeing the expected direct  $^1\text{H}$ - $^{13}\text{C}$  correlations, the correlation shown around 7.4 ppm in  $^1\text{H}$  dimension of the spectrum with a 2.0 ms contact time is assigned to the correlation between silanol group and the  $\epsilon\text{-CH}_2$  of adsorbed lysine. This result provides strong evidence that the side-chain amine group of adsorbed lysine interacts with silanol groups on silica surfaces and gets protonated.

The  $^{13}\text{C}$ ,  $^{15}\text{N}$ -lysine/ $\text{SiO}_2$  sample prepared in this work involves sodium chloride introduced by the pH adjustment process with NaOH during adsorption. The NaCl is difficult to remove because the solubility of lysine in water is similar to that of sodium chloride. To understand if sodium chloride will impact the lysine adsorption on silica surfaces, we carried out several experiments with natural abundance lysine that is initially salt free and applied  $^1\text{H} \rightarrow ^{13}\text{C}$  CP-MAS NMR spectroscopy to characterize the state of adsorbed lysine. The results are shown in Figure 8 for (a) Lys/ $\text{SiO}_2$ -0.01 M sample, (b) Lys/ $\text{SiO}_2$ -0.10 M sample, and (c) the sample prepared in a similar way as Lys/ $\text{SiO}_2$ -0.10 M sample with 0.20 M NaCl (Lys/ $\text{SiO}_2$ -0.10M/NaCl). On the basis of the NMR results, it is easy to determine that the salt-free Lys/ $\text{SiO}_2$ -0.10 M sample shows a small peak at 164 ppm that was not observed in the spectra of both the Lys/ $\text{SiO}_2$ -0.01 M and Lys/ $\text{SiO}_2$ -0.10M/NaCl samples. This is because lysine molecules form a monolayer on silica nanoparticles for Lys/ $\text{SiO}_2$ -0.01M/NaCl and Lys/ $\text{SiO}_2$ -0.10M/NaCl samples whereas they form multilayers for Lys/ $\text{SiO}_2$ -0.10 M sample. The resonance at 164 ppm is assigned to carbonyl carbon of carbamates because primary amines are known to be able to react with  $\text{CO}_2$  to form alkylammonium and alkylcarbamates according to a reaction shown

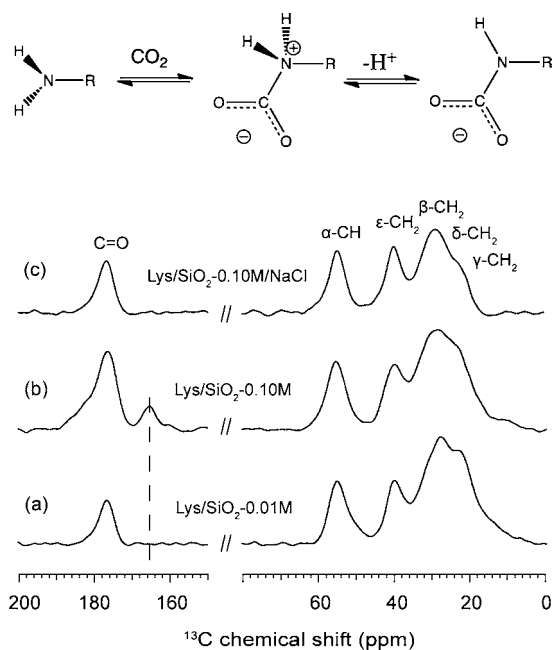


**Figure 8.**  $^1\text{H} \rightarrow ^{13}\text{C}$  CP-MAS NMR spectra of (a) Lys/ $\text{SiO}_2$ -0.01 M, (b) Lys/ $\text{SiO}_2$ -0.10M, and (c) Lys/ $\text{SiO}_2$ -0.10M/NaCl. The experiments were carried out at a  $^1\text{H}$  Larmor frequency of 400 MHz with a 4.0 mm triple-resonance probe operating in triple-resonance ( $^1\text{H}/^{13}\text{C}/^{15}\text{N}$ ) mode, a contact time of 1.0 ms, and a MAS speed of 10 kHz.

in Figure 8.<sup>68,73,74</sup> The formed carbamates can interact with adsorbed lysine in the salt-free system by forming hydrogen bonds with protonated  $\alpha\text{-NH}_3^+$ , making it detectable by  $^1\text{H} \rightarrow ^{13}\text{C}$  CP-MAS NMR spectroscopy. As a result, all amine groups of adsorbed lysine are protonated in the former case, preventing them from reacting with  $\text{CO}_2$  in air. After NaCl is introduced into Lys/ $\text{SiO}_2$ -0.10M, both sodium ions and chloride ions can break the hydrogen bonding system formed by carbamates and  $\alpha\text{-NH}_3^+$  of adsorbed lysine, making the small peak disappear. This point also agrees with the TGA result in which the surface coverage of sample (c) is about 1.60 molecules/ $\text{nm}^2$ . This is lower than the surface coverage of Lys/ $\text{SiO}_2$ -0.10 M sample (1.82 molecules/ $\text{nm}^2$ ). According to these two results, we conclude that sodium chloride decreased the amount of adsorbed lysine and it prevented lysine from forming multilayers on silica surfaces. The sample (c) is in fact a monolayer sample, where the surface coverage of lysine reaches the maximum for monolayer adsorption ( $\sim 1.60$  molecules/ $\text{nm}^2$ ).

**DFT Calculation.** To elucidate the adsorption state of lysine on silica surfaces and to determine the exact complex structure lysine forms with surface silanol group, we applied DFT calculations. Generally, we optimized structures and calculated the chemical shifts for bulk lysine and a possible lysine-silanol complex determined from NMR experiments (Figure 9). In this work, we extrapolated curves for  $^{13}\text{C}$  and  $^{15}\text{N}$  to convert all calculated chemical shielding values to chemical shift values. The extrapolated equation for  $^{13}\text{C}$  chemical shifts was derived based on the experimental and calculated  $^{13}\text{C}$  chemical shift values of bulk lysine because the structure of bulk lysine was elucidated in this work. Extrapolated equation of  $^{15}\text{N}$  chemical shift was obtained from the work of Dos et al.<sup>67,68</sup> because they studied the structure of poly-L-lysine systematically by  $^{15}\text{N}$

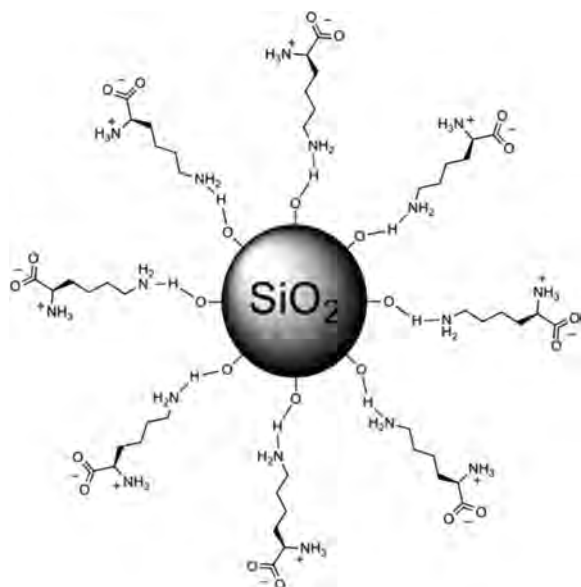


**Figure 9.** Schematic of the favorable model for lysine adsorption on fume silica nanoparticles surfaces.

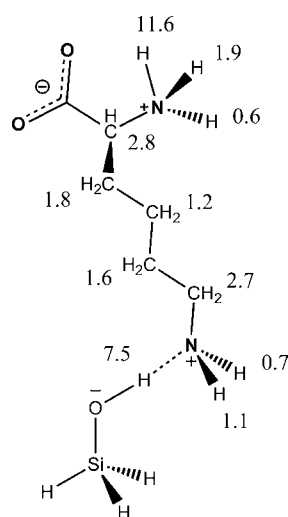
NMR and DFT calculations. The extrapolated equations of  $^{13}\text{C}$  and  $^{15}\text{N}$  chemical shifts are as follows:

$$^{13}\text{C}: \delta_{\text{extrapolate}} = -1.123 \cdot \sigma_{\text{cal}} + 206.1 \text{ ppm}$$

$$^{15}\text{N}: \delta_{\text{extrapolate}} = -0.778 \cdot \sigma_{\text{cal}} + 212.9 \text{ ppm}$$

Using these equations, all calculated  $^{13}\text{C}$  and  $^{15}\text{N}$  chemical shielding values were converted to chemical shift values (Table 3). It is found that the N–H distance in hydrogen bonding system is 1.807 Å for Lys-H-OSiH<sub>3</sub>, corresponding to a hydrogen bonding energy of 42.01 kJ/mol (see Table S1 of Supporting Information). From chemical shift calculations, the  $\alpha\text{-NH}_3^+$  protons of bulk lysine have three different chemical shifts at 11.6, 1.9, and 0.5 ppm due to the asymmetry of the protons. After the calculated chemical shifts are averaged, the average value (4.7 ppm) is still far from the experiment result. This is probably due to the fact that the  $\alpha\text{-NH}_3^+$  group may interact with other groups like the carboxylate group and Cl<sup>-</sup> ions or that the model used for calculation is not reliable enough to get reliable  $\alpha\text{-NH}_3^+$   $^1\text{H}$  chemical shifts.<sup>75</sup> For other groups, the  $^1\text{H}$  chemical shifts are very close to the experimental results. For Lys-H-OSiH<sub>3</sub>, the  $\epsilon\text{-NH}_3^+$  group

**Table 3.** Calculated  $^1\text{H}$ ,  $^{13}\text{C}$  and  $^{15}\text{N}$  Chemical Shielding Values and Extrapolated Chemical Shifts for Lysine and Lysine–Silanol Complex from DFT Calculations<sup>a</sup>



nucleus	group	lysine		LysH <sup>+</sup> OSiH <sub>3</sub>		
		calculated	experiment	calculated	extrapolated	experiment
$^{13}\text{C}$	C=O	26.0	177	26.0	177	177
	$\alpha\text{-CH}$	133.0	55	133.2	57	55
	$\beta\text{-CH}_2$	154.3	35	154.5	33	30
	$\gamma\text{-CH}_2$	162.2	22	162.4	24	23
	$\delta\text{-CH}_2$	155.4	32	158.4	28	27
	$\epsilon\text{-CH}_2$	145.3	44	146.7	41	40
$^{15}\text{N}$	$\alpha\text{-NH}_3^+$	226.3	39	226.7	37	39
	$\epsilon\text{-NH}_2/\epsilon\text{-NH}_3^+$	232.7	24	227.8	36	32
$^1\text{H}$	$\alpha\text{-CH}$	2.8	3.6	2.8	–	3.6
	$\beta\text{-CH}_2$	1.8	1.8	1.8	–	1.5
	$\gamma\text{-CH}_2$	1.2	1.5	1.2	–	1.2
	$\delta\text{-CH}_2$	1.5	2.0	1.6	–	1.5
	$\epsilon\text{-CH}_2$	2.8	2.2	2.7	–	2.6
	$\alpha\text{-NH}_3^+$	11.6, 1.9, 0.5	8.4	11.6, 1.9, 0.6	–	8.4
	$\epsilon\text{-NH}_2/\epsilon\text{-NH}_3^+$	0.7	–	7.5, 1.1, 0.7	–	7.4

<sup>a</sup>Chemical shifts are reported in ppm.

shows calculated chemical shifts of 7.5, 1.1, and 0.7 ppm where the hydrogen bonding proton has a chemical shift of 7.5 ppm. Considering the slow free rotation of the  $\epsilon$ -NH<sub>3</sub><sup>+</sup> group due to the strong hydrogen binding, the calculation result is consistent with the experimental result (7.4 ppm). Moreover, the calculated <sup>13</sup>C chemical shift of  $\epsilon$ -CH<sub>2</sub> for Lys-H-OSiH<sub>3</sub> is only 1 ppm off the experimental data and the calculated <sup>15</sup>N chemical shifts of  $\alpha$ -NH<sub>3</sub><sup>+</sup> and  $\epsilon$ -NH<sub>3</sub><sup>+</sup> are 2 and 4 ppm off the experimental data, respectively, for Lys-H-OSiH<sub>3</sub>. Combining the calculated and experimental results, it is convincing to argue that the lysine side-chain amine group is the dominant hydrogen-bonding interaction with surface silanol groups at silica nanoparticles and that the Lys-H-OSiH<sub>3</sub> complex is the most probable structure. These results are combined with NMR experiment results, and the proposed favorable model for lysine adsorption on fumed silica nanoparticle surfaces is presented in Figure 9.

## CONCLUSION

The structure of bulk lysine and lysine adsorbed on fumed silica nanoparticles was thoroughly investigated by ultrafast MAS <sup>1</sup>H, <sup>13</sup>C, and <sup>15</sup>N NMR spectroscopy. Bulk L-lysine has protonated  $\alpha$ -NH<sub>3</sub><sup>+</sup> and deprotonated  $\epsilon$ -NH<sub>2</sub>. Lysine adsorbed on fumed silica nanoparticles from solution interacts with silica surfaces through hydrogen bonding between side-chain amine groups and surface silanol groups. When the spectroscopy results were combined with DFT calculations, we further proposed that the Lys-H-OSiH<sub>3</sub> complex is the favorable model for the lysine adsorption state on silica surfaces. The proposed model can be used to elucidate the mechanism of synthesizing ultrasmall silica nanoparticles (~10 nm) with lysine as capping ligands, and it is of use to researchers interested in surface functionalization and modification. Also, the agreement between DFT calculated and experimentally determined NMR chemical shifts is in general quite good, indicating that the combination of solid-state NMR and DFT chemical shift calculations can indeed be used to study surface chemistry at the interface of biomolecules and nanoparticles.

## ASSOCIATED CONTENT

### Supporting Information

<sup>1</sup>H-<sup>13</sup>C HETCOR NMR spectrum of bulk lysine; 2D <sup>13</sup>C-<sup>13</sup>C INADEQUATE NMR spectrum of <sup>13</sup>C,<sup>15</sup>N-lysine·2HCl; <sup>15</sup>N-<sup>13</sup>C 2D HETCOR NMR spectrum of <sup>13</sup>C,<sup>15</sup>N-lysine/SiO<sub>2</sub>; 2D <sup>13</sup>C-<sup>13</sup>C through-space correlation NMR spectrum of <sup>13</sup>C,<sup>15</sup>N-lysine·2HCl; extrapolated curve of <sup>13</sup>C chemical shift; and summary of lysine-silanol complex from DFT calculations. This material is available free of charge via the Internet at <http://pubs.acs.org>.

## AUTHOR INFORMATION

### Corresponding Author

\*E-mail: [gholland@mail.sdsu.edu](mailto:gholland@mail.sdsu.edu).

### Notes

The authors declare no competing financial interest.

## ACKNOWLEDGMENTS

The research was supported by grants from the National Science Foundation (CHE-1011937). We thank Dr. Brian Cherry for help with NMR instrumentation, student training, and scientific discussion.

## REFERENCES

- (1) Lambert, J. F. Adsorption and Polymerization of Amino Acids on Mineral Surfaces: A Review. *Origins Life Evol. Biospheres* **2008**, *38*, 211–242.
- (2) Lambert, J. F.; Stievano, L.; Lopes, I.; Gharsallah, M.; Piao, L. The Fate of Amino Acids Adsorbed on Mineral Matter. *Planet. Space Sci.* **2009**, *57*, 460–467.
- (3) Zaia, D. A. M. A Review of Adsorption of Amino Acids on Minerals: Was It Important for Origin of Life? *Amino Acids* **2004**, *27*, 113–118.
- (4) Tarn, D.; Ashley, C. E.; Xue, M.; Carnes, E. C.; Zink, J. I.; Brinker, C. J. Mesoporous Silica Nanoparticle Nanocarriers: Biofunctionality and Biocompatibility. *Acc. Chem. Res.* **2013**, *46*, 792–801.
- (5) Malfatti, M. A.; Palko, H. A.; Kuhn, E. A.; Turteltaub, K. W. Determining the Pharmacokinetics and Long-Term Biodistribution of SiO<sub>2</sub> Nanoparticles in Vivo Using Accelerator Mass Spectrometry. *Nano Lett.* **2012**, *12*, 5532–5538.
- (6) Zhang, H.; Dunphy, D. R.; Jiang, X.; Meng, H.; Sun, B.; Tarn, D.; Xue, M.; Wang, X.; Lin, S.; Ji, Z.; et al. Processing Pathway Dependence of Amorphous Silica Nanoparticle Toxicity: Colloidal vs Pyrolytic. *J. Am. Chem. Soc.* **2012**, *134*, 15790–15804.
- (7) Graf, C.; Gao, Q.; Schütz, I.; Noufele, C. N.; Ruan, W.; Posselt, U.; Korotianskiy, E.; Nordmeyer, D.; Rancan, F.; Hadam, S.; et al. Surface Functionalization of Silica Nanoparticles Supports Colloidal Stability in Physiological Media and Facilitates Internalization in Cells. *Langmuir* **2012**, *28*, 7598–7613.
- (8) Ashley, C. E.; Carnes, E. C.; Epler, K. E.; Padilla, D. P.; Phillips, G. K.; Castillo, R. E.; Wilkinson, D. C.; Wilkinson, B. S.; Burgard, C. A.; Kalinich, R. M.; et al. Delivery of Small Interfering RNA by Peptide-Targeted Mesoporous Silica Nanoparticle-Supported Lipid Bilayers. *ACS Nano* **2012**, *6*, 2174–2188.
- (9) Patwardhan, S. V.; Emami, F. S.; Berry, R. J.; Jones, S. E.; Naik, R. R.; Deschaume, O.; Heinz, H.; Perry, C. C. Chemistry of Aqueous Silica Nanoparticle Surfaces and the Mechanism of Selective Peptide Adsorption. *J. Am. Chem. Soc.* **2012**, *134*, 6244–6256.
- (10) Hubbell, J. A.; Chilkoti, A. Nanomaterials for Drug Delivery. *Science* **2012**, *337*, 303–305.
- (11) Ashley, C. E.; Carnes, E. C.; Phillips, G. K.; Padilla, D.; Durfee, P. N.; Brown, P. A.; Hanna, T. N.; Liu, J.; Phillips, B.; Carter, M. B.; et al. The Targeted Delivery of Multicomponent Cargos to Cancer Cells by Nanoporous Particle-Supported Lipid Bilayers. *Nat. Mater.* **2011**, *10*, 389–397.
- (12) Liu, J.; Stace-Naughton, A.; Jiang, X.; Brinker, C. J. Porous Nanoparticle Supported Lipid Bilayers (Protocells) as Delivery Vehicles. *J. Am. Chem. Soc.* **2009**, *131*, 1354–1355.
- (13) Vallet-Regi, M.; Rámila, A.; del Real, R. P.; Perez-Pariente, J. A. New Property of MCM-41: Drug Delivery System. *Chem. Mater.* **2001**, *13*, 308–311.
- (14) Lu, J.; Liong, M.; Zink, J. I.; Tamanoi, F. Mesoporous Silica Nanoparticles as a Delivery System for Hydrophobic Anticancer Drugs. *Small* **2007**, *3*, 1341–1346.
- (15) Orgel, L. E. Polymerization on the Rocks: Theoretical Introduction. *Origins Life Evol. Biospheres* **1998**, *28*, 227–234.
- (16) Rimola, A.; Costa, D.; Sodupe, M.; Lambert, J. F.; Ugliengo, P. Silica Surface Features and Their Role in the Adsorption of Biomolecules: Computational Modeling and Experiments. *Chem. Rev. (Washington, DC, U.S.)* **2013**, *113*, 4216–4313.
- (17) Liu, C. C.; Maciel, G. E. The Fumed Silica Surface: A Study by NMR. *J. Am. Chem. Soc.* **1996**, *118*, 5103–5119.
- (18) McDonald, R. S. Surface Functionality of Amorphous Silica by Infrared Spectroscopy. *J. Phys. Chem.* **1958**, *62*, 1168–1178.
- (19) Morrow, B. A.; McFarlan, A. J. Surface Vibrational Modes of Silanol Groups on Silica. *J. Phys. Chem.* **1992**, *96*, 1395–1400.
- (20) Gunko, V. M.; Voronin, E. F.; Pakhlov, E. M.; Zarko, V. I.; Turov, V. V.; Guzenko, N. V.; Lebeda, R. Features of Fumed Silica Coverage with Silanes Having Three or Two Groups Reacting with the Surface. *Colloids Surf., A* **2000**, *166*, 187–201.



- (21) Bakaev, V. A.; Pantano, C. G. Inverse Reaction Chromatography. 2. Hydrogen/Deuterium Exchange with Silanol Groups on the Surface of Fumed Silica. *J. Phys. Chem. C* **2009**, *113*, 13894–13898.
- (22) Peng, L.; Qisui, W.; Xi, L.; Chaocan, Z. Investigation of the States of Water and OH Groups on the Surface of Silica. *Colloids Surf, A* **2009**, *334*, 112–115.
- (23) Tielens, F.; Gervais, C.; Lambert, J. F.; Mauri, F.; Costa, D. Ab Initio Study of the Hydroxylated Surface of Amorphous Silica: A Representative Model. *Chem. Mater.* **2008**, *20*, 3336–3344.
- (24) Aboshi, A.; Kurumoto, N.; Yamada, T.; Uchino, T. Influence of Thermal Treatments on the Photoluminescence Characteristics of Nanometer-Sized Amorphous Silica Particles. *J. Phys. Chem. C* **2007**, *111*, 8483–8488.
- (25) Brei, V. V. <sup>29</sup>Si Solid-State NMR Study of the Surface Structure of Aerosil Silica. *J. Chem. Soc. Faraday Trans.* **1994**, *90*, 2961–2964.
- (26) Tomczak, M. M.; Glawe, D. D.; Drummy, L. F.; Lawrence, C. G.; Stone, M. O.; Perry, C. C.; Pochan, D. J.; Deming, T. J.; Naik, R. R. Polypeptide-Templated Synthesis of Hexagonal Silica Platelets. *J. Am. Chem. Soc.* **2005**, *127*, 12577–12582.
- (27) Yokoi, T.; Sakamoto, Y.; Terasaki, O.; Kubota, Y.; Okubo, T.; Tatsumi, T. Periodic Arrangement of Silica Nanospheres Assisted by Amino Acids. *J. Am. Chem. Soc.* **2006**, *128*, 13664–13665.
- (28) Yokoi, T.; Wakabayashi, J.; Otsuka, Y.; Fan, W.; Iwama, M.; Watanabe, R.; Aramaki, K.; Shimojima, A.; Tatsumi, T.; Okubo, T. Mechanism of Formation of Uniform-Sized Silica Nanospheres Catalyzed by Basic Amino Acids. *Chem. Mater.* **2009**, *21*, 3719–3729.
- (29) Behrens, S. H.; Grier, D. G. The Charge of Glass and Silica Surfaces. *J. Chem. Phys.* **2001**, *115*, 6716–6721.
- (30) Roddick-Lanzilotta, A. D.; Connor, P. A.; McQuillan, A. J. An In Situ Infrared Spectroscopic Study of the Adsorption of Lysine to TiO<sub>2</sub> from an Aqueous Solution. *Langmuir* **1998**, *14*, 6479–6484.
- (31) Kitadai, N.; Yokoyama, T.; Nakashima, S. In Situ ATR-IR Investigation of L-Lysine Adsorption on Montmorillonite. *J. Colloid Interface Sci.* **2009**, *338*, 395–401.
- (32) Wright, D. A.; Marsh, R. E. The Crystal Structure of L-Lysine Monohydrochloride Dihydrate. *Acta Crystallogr.* **1962**, *15*, 54–64.
- (33) Koetzle, T. F.; Lehmann, M. S.; Verbist, J. J.; Hamilton, W. C. Precision Neutron Diffraction Structure Determination of Protein and Nucleic Acid Components. VII. The Crystal and Molecular Structure of the Amino Acid L-Lysine Monohydrochloride Dihydrate. *Acta Crystallogr.* **1972**, *B28*, 3207–3214.
- (34) Ben Shir, I.; Kababya, S.; Schmidt, A. Binding Specificity of Amino Acids to Amorphous Silica Surfaces: Solid-State NMR of Glycine on SBA-15. *J. Phys. Chem. C* **2012**, *116*, 9691–9702.
- (35) Amitay-Rosen, T.; Vega, S. A Deuterium MAS NMR Study of the Local Mobility of Dissolved Methionine and Di-Alanine at the Inner Surface of SBA-15. *Phys. Chem. Chem. Phys.* **2010**, *12*, 6763–6773.
- (36) Amitay-Rosen, T.; Kababya, S.; Vega, S. A Dynamic Magic Angle Spinning NMR Study of the Local Mobility of Alanine in an Aqueous Environment at the Inner Surface of Mesoporous Materials. *J. Phys. Chem. B* **2009**, *113*, 6267–6282.
- (37) Gao, Q.; Xu, W.; Xu, Y.; Wu, D.; Sun, Y.; Deng, F.; Shen, W. Amino Acid Adsorption on Mesoporous Materials: Influence of Types of Amino Acids, Modification of Mesoporous Materials, and Solution Conditions. *J. Phys. Chem. B* **2008**, *112*, 2261–2267.
- (38) Stievano, L.; Yu Piao, L.; Lopes, I.; Meng, M.; Costa, D.; Lambert, J. F. Glycine and Lysine Adsorption and Reactivity on the Surface of Amorphous Silica. *Eur. J. Mineral.* **2007**, *19*, 321–331.
- (39) Meng, M.; Stievano, L.; Lambert, J. F. Adsorption and Thermal Condensation Mechanisms of Amino Acids on Oxide Supports. 1. Glycine on Silica. *Langmuir* **2004**, *20*, 914–923.
- (40) Lopes, I.; Piao, L.; Stievano, L.; Lambert, J. F. Adsorption of Amino Acids on Oxide Supports: A Solid-State NMR Study of Glycine Adsorption on Silica and Alumina. *J. Phys. Chem. C* **2009**, *113*, 18163–18172.
- (41) Kitadai, N.; Yokoyama, T.; Nakashima, S. ATR-IR Spectroscopic Study of L-Lysine Adsorption on Amorphous Silica. *J. Colloid Interface Sci.* **2009**, *329*, 31–37.
- (42) O'Connor, A. J.; Hokura, A.; Kisler, J. M.; Shimazu, S.; Stevens, G. W.; Komatsu, Y. Amino Acid Adsorption onto Mesoporous Silica Molecular Sieves. *Sep. Purif. Technol.* **2006**, *48*, 197–201.
- (43) Vlasova, N. N.; Golovkova, L. P. The Adsorption of Amino Acids on the Surface of Highly Dispersed Silica. *Colloid J.* **2004**, *66*, 657–662.
- (44) Dybowski, C.; Bai, S. Solid-State NMR Spectroscopy. *Anal. Chem.* **2008**, *80*, 4295–4300.
- (45) Ben Shir, I.; Kababya, S.; Amitay-Rosen, T.; Balazs, Y. S.; Schmidt, A. Molecular Level Characterization of the Inorganic–Bioorganic Interface by Solid State NMR: Alanine on a Silica Surface, a Case Study. *J. Phys. Chem. B* **2010**, *114*, 5989–5996.
- (46) Mirau, P. A.; Serres, J. L.; Lyons, M. The Structure and Dynamics of Poly(L-Lysine) in Templated Silica Nanocomposites. *Chem. Mater.* **2008**, *20*, 2218–2223.
- (47) Gullion, T.; Schaefer, J. Rotational-Echo Double-Resonance NMR. *J. Magn. Reson.* **1989**, *81*, 196–200.
- (48) Ben Shir, I.; Kababya, S.; Schmidt, A. Molecular Details of Amorphous Silica Surfaces Determine Binding Specificity to Small Amino Acids. *J. Phys. Chem. C* **2014**, *118*, 7901–7909.
- (49) Andrew, E. R. The Narrowing of NMR Spectra of Solids by High-Speed Specimen Rotation and the Resolution of Chemical Shift and Spin Multiplet Structures for Solids. *Prog. Nucl. Magn. Reson. Spectrosc.* **1971**, *8*, 1–39.
- (50) Brown, S. P. Probing Proton–Proton Proximities in the Solid State. *Prog. Nucl. Magn. Reson. Spectrosc.* **2007**, *50*, 199–251.
- (51) Brown, S. P. Applications of High-Resolution <sup>1</sup>H Solid-State NMR. *Solid State Nucl. Magn. Reson.* **2012**, *41*, 1–27.
- (52) Hohenberg, P.; Kohn, W. Inhomogeneous Electron Gas. *Phys. Rev.* **1964**, *136*, 864–871.
- (53) Kohn, W.; Sham, L. J. Self-Consistent Equations Including Exchange and Correlation Effects. *Phys. Rev.* **1965**, *140*, 1133–1138.
- (54) Hartmann, S. R.; Hahn, E. L. Nuclear Double Resonance in the Rotating Frame. *Phys. Rev.* **1962**, *128*, 2042–2053.
- (55) Meier, B. H. Cross Polarization under Fast Magic Angle Spinning: Thermodynamical Considerations. *Chem. Phys. Lett.* **1992**, *18*, 201–207.
- (56) Takegoshi, K.; Nakamura, S.; Terao, T. <sup>13</sup>C–<sup>1</sup>H Dipolar-Assisted Rotational Resonance in Magic-Angle Spinning NMR. *Chem. Phys. Lett.* **2001**, *344*, 631–637.
- (57) Takegoshi, K.; Nakamura, S.; Terao, T. <sup>13</sup>C–<sup>1</sup>H Dipolar-Driven <sup>13</sup>C–<sup>13</sup>C Recoupling without <sup>13</sup>C RF Irradiation in Nuclear Magnetic Resonance of Rotating Solids. *J. Chem. Phys.* **2003**, *118*, 2325–2341.
- (58) Lesage, A.; Auger, C.; Caldarelli, S.; Emsley, L. Determination of Through-Bond Carbon–Carbon Connectivities in Solid-State NMR Using the INADEQUATE Experiment. *J. Am. Chem. Soc.* **1997**, *119*, 7867–7868.
- (59) Lesage, A.; Bardet, M.; Emsley, L. Through-Bond Carbon–Carbon Connectivities in Disordered Solids by NMR. *J. Am. Chem. Soc.* **1999**, *121*, 10987–10993.
- (60) Bennett, A. E.; Rienstra, C. M.; Auger, M.; Lakshmi, K. V.; Griffin, R. G. Heteronuclear Decoupling in Rotating Solids. *J. Chem. Phys.* **1995**, *103*, 6951–6958.
- (61) Feike, M.; Demco, D. E.; Graf, R.; Gottwald, J.; Hafner, S.; Spiess, H. W. Broadband Multiple-Quantum NMR Spectroscopy. *J. Magn. Reson., Ser. A* **1996**, *122*, 214–221.
- (62) Feike, M.; Graf, R.; Schnell, I.; Jager, C.; Spiess, H. W. Structure of Crystalline Phosphates From <sup>31</sup>P Double-Quantum NMR Spectroscopy. *J. Am. Chem. Soc.* **1996**, *118*, 9631–9634.
- (63) Schnell, I.; Spiess, H. W. High-Resolution <sup>1</sup>H NMR Spectroscopy in the Solid State: Very Fast Sample Rotation and Multiple-Quantum Coherences. *J. Magn. Reson.* **2001**, *151*, 153–227.
- (64) Hayashi, S.; Hayamizu, K. Chemical Shift Standards in High-Resolution Solid-State NMR (1) <sup>13</sup>C, <sup>29</sup>Si, and <sup>1</sup>H Nuclei. *Bull. Chem. Soc. Jpn.* **1991**, *64*, 685–687.
- (65) Hayashi, S.; Hayamizu, K. Chemical Shift Standards in High-Resolution Solid-State NMR (2) <sup>15</sup>N Nuclei. *Bull. Chem. Soc. Jpn.* **1991**, *64*, 688–690.

(66) Becke, A. D. Density-Functional Thermochemistry. III. the Role of Exact Exchange. *J. Chem. Phys.* **1993**, *98*, 5648–5652.

(67) Dos, A.; Schimming, V.; Huot, M. C.; Limbach, H. H. Acid-Induced Amino Side-Chain Interactions and Secondary Structure of Solid Poly-L-Lysine Probed by  $^{15}\text{N}$  and  $^{13}\text{C}$  Solid State NMR and Ab Initio Model Calculations. *J. Am. Chem. Soc.* **2009**, *131*, 7641–7653.

(68) Dos, A.; Schimming, V.; Tosoni, S.; Limbach, H. H. Acid-Base Interactions and Secondary Structures of Poly-L-Lysine Probed by  $^{15}\text{N}$  and  $^{13}\text{C}$  Solid State NMR and Ab Initio Model Calculations. *J. Phys. Chem. B* **2008**, *112*, 15604–15615.

(69) Rimola, A.; Sodupe, M.; Ugliengo, P. Affinity Scale for the Interaction of Amino Acids with Silica Surfaces. *J. Phys. Chem. C* **2009**, *113*, 5741–5750.

(70) Wolinski, K.; Hinton, J. F.; Pulay, P. Efficient Implementation of the Gauge-Independent Atomic Orbital Method for NMR Chemical Shift Calculations. *J. Am. Chem. Soc.* **1990**, *112*, 8251–8260.

(71) Schreckenbach, G.; Ziegler, T. Calculation of NMR Shielding Tensors Using Gauge-Including Atomic Orbitals and Modern Density Functional Theory. *J. Phys. Chem.* **1995**, *99*, 606–611.

(72) Manriquez, R.; López-Dellamary, F. A.; Frydel, J.; Emmler, T.; Breitzke, H.; Buntkowsky, G.; Limbach, H. H.; Shenderovich, I. G. Solid-State NMR Studies of Aminocarboxylic Salt Bridges in L-Lysine Modified Cellulose. *J. Phys. Chem. B* **2009**, *113*, 934–940.

(73) Maeda, S.; Oumae, S.; Kaneko, S.; Kunitomo, K.-K. Formation of Carbamates and Cross-Linking of Microbial Poly( $\epsilon$ -L-Lysine) Studied by  $^{13}\text{C}$  and  $^{15}\text{N}$  Solid-State NMR. *Polym. Bull.* **2011**, *68*, 745–754.

(74) Schimming, V.; Hoelger, C. G.; Buntkowsky, G.; Sack, I.; Fuhrhop, J. H.; Rocchetti, S.; Limbach, H. H. Evidence by  $^{15}\text{N}$  CPMAS and  $^{15}\text{N}$ – $^{13}\text{C}$  REDOR NMR for Fixation of Atmospheric  $\text{CO}_2$  by Amino Groups of Biopolymers in the Solid State. *J. Am. Chem. Soc.* **1999**, *121*, 4892–4893.

(75) Schmidt, J.; Hoffmann, A.; Spiess, H. W.; Sebastiani, D. Bulk Chemical Shifts in Hydrogen-Bonded Systems from First-Principles Calculations and Solid-State-NMR. *J. Phys. Chem. B* **2006**, *110*, 23204–23210.